

# COAD: Constant-Time Planning for Continuous Goal Manipulation with Compressed Library and Online Adaptation

Adil Shiyas\*, Zhuoyun Zhong\*, and Constantinos Chamzas

**Abstract**—In many robotic manipulation tasks, the robot repeatedly solves motion-planning problems that differ mainly in the location of the goal object and its associated obstacle, while the surrounding workspace remains fixed. Prior works have shown that leveraging experience and offline computation can accelerate repeated planning queries, but they lack guarantees of covering the continuous task space and require storing large libraries of solutions. In this work, we present COAD, a framework that provides constant-time planning over a continuous goal-parameterized task space. COAD discretizes the continuous task space into finitely many Task Coverage Regions. Instead of planning and storing solutions for every region offline, it constructs a compressed library by only solving representative root problems. Other problems are handled through fast adaptation from these root solutions. At query time, the system retrieves a root motion in constant time and adapts it to the desired goal using lightweight adaptation modules such as linear interpolation, Dynamic Movement Primitives, or simple trajectory optimization. We evaluate the framework on various manipulators and environments in simulation and the real world, showing that COAD achieves substantial compression of the motion library while maintaining high success rates and sub-millisecond-level queries, outperforming baseline methods in both efficiency and path quality. The source code is available at <https://github.com/elpis-lab/CoAd>

## I. INTRODUCTION

Motion planning is a central problem in robotics, enabling autonomous systems to plan collision-free motions while satisfying kinematic and geometric constraints [1]. In robotic manipulation, this problem becomes particularly challenging due to high-dimensional configuration spaces, complex robot geometry, and cluttered workspaces. Despite these challenges, significant progress has been made over the years [2], and recent efforts have focused on leveraging experience and pre-computation to accelerate repeated queries [3].

Library-based [4] and experience-driven planners [5] store and adapt previously computed solutions, often achieving substantial speedups in structured settings. However, despite their practical effectiveness, these approaches typically provide no guarantees that all task instances drawn from a continuous distribution will be solvable.

In this work, we consider a structured yet practically important setting in which the distribution of planning problems is known. Specifically, we study manipulation tasks such as the tabletop picking scenario shown in Fig. 1, where a robot must repeatedly grasp a known object placed at varying poses while other workspace obstacles remain fixed. Such

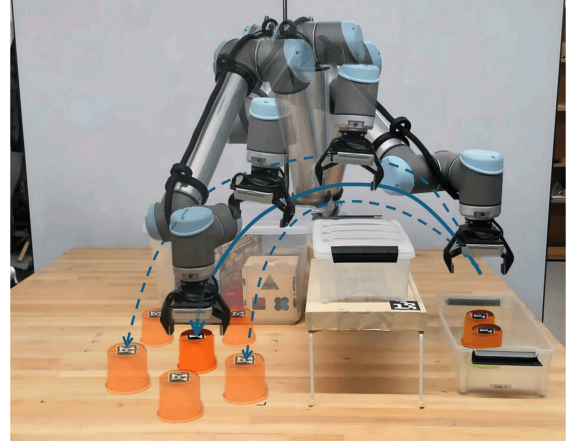


Fig. 1: A physical UR10 robot repeatedly solves motion-planning problems to grasp an object whose pose continuously varies across queries, while the rest of the workspace remains unchanged.

settings commonly arise in production workcells for tasks such as kitting, packaging, and pick-and-place. We refer to this family of problems as **goal-varying motion planning**, where each planning query differs only in the pose of a known object within a bounded region of  $SE(3)$ .

Although this setting appears simple, it still induces an infinite family of motion planning problems due to the *continuous goal pose*. COAD addresses this by leveraging the following key property: if a path is valid for a nominal object pose and remains valid under bounded perturbations of that pose, then that single path certifies feasibility for an entire continuous subset of nearby object placements. This property allows the continuous goal space to be covered by finitely many regions, where a single path certifies feasibility for all goals within each region. Furthermore, rather than computing a distinct motion plan for every region, COAD constructs a *compressed library* of root paths. The remaining regions are handled through fast *adaptation* of these root paths toward their region goals, while preserving feasibility within their certified coverage. At query time, COAD identifies the region containing the query goal, retrieves the corresponding root path from library, and adapts it online to the region goal.

To the best of our knowledge, this is the first framework that provides constant-time guarantees for continuous goal-parameterized motion planning domains. Prior constant-time approaches assume a discrete representation of the goal space [6]. Concretely, our contributions are:

- We present a partitioning framework that enumerates an infinite family of planning queries to a finite set of paths, each associated with a certified region of goal poses.

All authors are affiliated with the Department of Robotics Engineering, Worcester Polytechnic Institute (WPI), Worcester, MA 01609, USA {mshiyas, zzhong3, cchamzas}@wpi.edu.

\* Adil Shiyas and Zhuoyun Zhong have equal contributions.

- We propose an adaptation framework that deforms root paths toward new goal poses while preserving feasibility within their certified regions, enabling efficient storage and reuse of prior paths.
- We demonstrate the effectiveness of COAD on manipulation tasks with 7-DOF and 8-DOF manipulators, showing compression of up to 97% of the full path library while achieving query times as low as 0.03 ms.

## II. RELATED WORK

### A. Classical Motion Planning

Motion planning has been studied extensively for several decades. Existing planners broadly fall into three categories. Sampling-based motion planners (SBMPs), such as PRM [7] and RRT-Connect [8], are *probabilistically complete*: if a solution exists, they will find it with probability one as the computation time approaches infinity. However, they provide no deterministic runtime guarantees. Graph-based planners are *resolution complete*, guaranteeing a solution at a fixed discretization resolution, but they scale poorly in high-dimensional manipulation spaces. Optimization-based planners [9], [10] often achieve fast performance in practice but lack global guarantees and may converge to local minima. While these methods are general-purpose and applicable to arbitrary motion planning problems, they do not provide guarantees over structured families of problems drawn from a continuous task distribution.

### B. Experience-Based Motion Planning

Experience-based motion planning seeks to accelerate repeated queries by equipping robots with memory and reusing prior solutions in related environments. Rather than planning from scratch, these methods retrieve and adapt stored trajectories [3], [4], [11], roadmaps [5], or learned sampling strategies [12]. Such approaches have demonstrated substantial speedups in challenging manipulation tasks. However, they typically assume that future planning queries are drawn from an unknown distribution and do not provide guarantees that accumulated experience will cover all admissible problem instances. As a result, they rely on fallback planners to ensure robustness.

### C. Constant-Time and Precomputation-Based Planning

More closely related to our work are fixed-time motion planning approaches [6], [13]–[15], which shift computational effort to an offline phase in order to guarantee bounded query-time performance. These methods pre-compute solutions for a finite set of task or obstacle configurations and retrieve appropriate trajectories at runtime. While they provide strong runtime guarantees, their results rely on a pre-discretized task space. In contrast, our framework provides constant-time guarantees over a continuous goal-parameterized domain. The work from [14] also operates in continuous spaces, but focuses on movable obstacles while the goal is fixed. We focus on the complementary problem where the goal is varied.

## III. NOTATIONS AND PROBLEM STATEMENT

Let  $q \in \mathcal{C}$  denote the configuration and configuration space of a robot. Let  $\mathcal{C}_{\text{obs}}$  denote the obstacle (invalid) configuration space, and denote the collision-free space as  $\mathcal{C}_{\text{free}} = \mathcal{C} \setminus \mathcal{C}_{\text{obs}}$ .

### A. Motion Planning Problem

Given a start configuration  $q_{\text{start}} \in \mathcal{C}_{\text{free}}$  and a goal region  $\mathcal{C}_{\text{goal}} \subseteq \mathcal{C}_{\text{free}}$ , motion planning problem tries to find a continuous path  $\pi : [0, 1] \rightarrow \mathcal{C}_{\text{free}}$  such that  $\pi(0) = q_{\text{start}}$ ,  $\pi(1) \in \mathcal{C}_{\text{goal}}$ .

### B. Goal-varying motion planning problem

In this work, we study a class of manipulation planning problems in which the goal depends on the pose of a movable object. Let  $\mathbf{T}_o \in \mathcal{T} \subseteq SE(3)$  denote the pose of a target object  $o$ , whose placement varies across queries within the bounded task space  $\mathcal{T}$  while the environment remains static. Such settings are common in tasks such as robotic grasping, where the robot must reach a grasp pose relative to the object (Fig. 1). For each object pose  $\mathbf{T}_o$ , the task induces a goal region in the robot configuration space, denoted  $\mathcal{C}_{\text{goal}}(\mathbf{T}_o)$ . Because the object itself occupies space in the workspace, its pose also affects the set of valid robot configurations. Consequently, the collision-free configuration space becomes object-dependent and is denoted  $\mathcal{C}_{\text{free}}(\mathbf{T}_o)$ .

Given an object pose  $\mathbf{T}_o \in \mathcal{O}$ , a start configuration  $q_{\text{start}} \in \mathcal{C}_{\text{free}}(\mathbf{T}_o)$  and a goal region  $\mathcal{C}_{\text{goal}}(\mathbf{T}_o)$ , we aim to compute a continuous path  $\pi : [0, 1] \rightarrow \mathcal{C}_{\text{free}}(\mathbf{T}_o)$  such that  $\pi(0) = q_{\text{start}}$ ,  $\pi(1) \in \mathcal{C}_{\text{goal}}(\mathbf{T}_o)$ , if such a path exists. We denote the family of these problems as:

$$p(\mathcal{T}) = \{(q_{\text{start}}, \mathcal{C}_{\text{goal}}(\mathbf{T}_o), \mathcal{C}_{\text{free}}(\mathbf{T}_o)) \mid \mathbf{T}_o \in \mathcal{T}\}$$

where both the goal region and the collision-free space vary continuously with  $\mathbf{T}_o$ .

## IV. METHODOLOGY

Since the set of motion planning problems  $p(\mathcal{T})$  contains infinitely many instances, computing a unique path for each is infeasible. Instead, we leverage the observation that a single path can remain valid for a continuous subset of object poses.

In Sec. IV-A, we show how this property allows us to partition the task space into a finite set of regions. In Sec. IV-B and Sec. IV-C, we describe how COAD leverages these finite regions to construct a motion-plan library that covers the entire domain. Finally, we show in Sec. IV-D that it enables constant-time solution for any problem  $\mathbf{T}_o \in \mathcal{T}$ . The overall framework is illustrated in Fig. 2.

### A. Task Space Discretization

1) *Task Space Region*: We begin by describing the goal regions  $\mathcal{C}_{\text{goal}}(\mathbf{T}_o)$  induced by the pose of the object using the *Task Space Regions* (TSRs) [16]. A TSR defines a set of admissible end-effector poses relative to an object that are valid for completing the task (e.g., grasping), as in Fig. 3 (a).

Formally, let  $\mathbf{T}_\delta \in SE(3)$  denote a displacement transform bounded by a box  $\mathbf{B} \subset \mathbb{R}^6$  specifying translational and rotational limits. The resulting displacement set is denoted

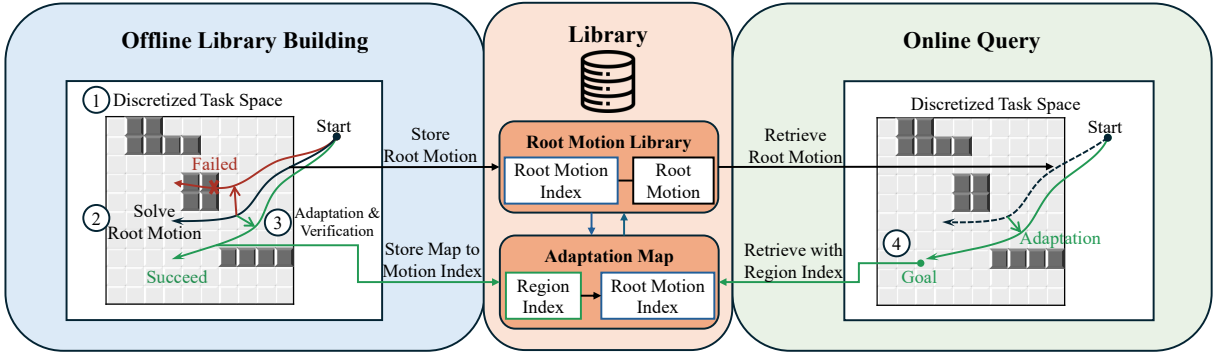


Fig. 2: COAD consists of an offline library-building stage and an online query stage. 1) The continuous task space is discretized into a finite set of TCRs, each indexed for constant-time lookup. 2) During offline preprocessing, an uncovered region is selected, a motion planner finds a *root motion* for that region, and the resulting path is stored in the root-motion library. 3) The same root motion is then adapted and verified on neighboring regions; successful adaptations are recorded in an adaptation map that links each covered region index to a root-motion index. 4) During the online query stage, the sensed Goal pose is mapped to its region index, the corresponding root motion is retrieved in constant time, and the motion is adapted to satisfy the queried goal condition using an adaption algorithm. This process yields a compressed library that provides constant plans and covers the full task space.

$\Delta(\mathbf{B})$ . Let  $\mathbf{T}_s \in SE(3)$  denote a fixed end-effector offset relative to the object frame, and let  $\mathbf{T}_o$  denote the pose of object  $o$ . The corresponding TSR is defined as:

$$\text{TSR}(\mathbf{T}_p) = \{\mathbf{T}_e \mid \exists \mathbf{T}_\delta \in \Delta(\mathbf{B}) \text{ s.t. } \mathbf{T}_e = \mathbf{T}_o \mathbf{T}_\delta \mathbf{T}_s\}. \quad (1)$$

Geometrically, the TSR is generated by allowing the local offset pose  $\mathbf{T}_\delta$  to vary over a 6-dimensional box, and mapping each such offset to an end-effector pose via rigid body transformations  $\mathbf{T}_e = \mathbf{T}_p \mathbf{T}_\delta \mathbf{T}_s$ . Thus, in the local coordinates of  $\mathbf{T}_\delta$ , the TSR is exactly a box-shaped region. The goal region in configuration space is therefore:

$$\mathcal{C}_{\text{goal}}(\mathbf{T}_o) = \{q \mid \text{FK}(q) \in \text{TSR}(\mathbf{T}_p)\}, \quad (2)$$

where FK denotes the forward kinematics of the robot.

2) *Shared goals across object poses*: Consider two object poses  $\mathbf{T}_{o1}$  and  $\mathbf{T}_{o2}$  whose TSRs overlap, as illustrated in Fig. 3 (b). In this case, there exists an end-effector pose  $\mathbf{T}_e$  that lies in the intersection of the two TSRs and therefore constitutes a valid goal for both object placements.

More importantly, because the TSR varies continuously with the object pose, this shared end-effector pose remains valid for all intermediate object poses along any continuous transformation from  $\mathbf{T}_{o1}$  to  $\mathbf{T}_{o2}$ , as illustrated in Fig. 3(c). This observation implies that a single end-effector goal can be valid for continuous subset of object poses.

3) *Task Coverage Regions*: Motivated by this observation, we introduce the notion of a Task Coverage Region (TCR). Rather than associating each object pose with a set of valid end-effector poses (as in TSRs), we invert this relationship and define the set of object poses that a fixed end-effector pose can solve.

**Definition 1.** (*Task Coverage Region*):

Given a TSR with  $\mathbf{T}_\delta$ ,  $\Delta(\mathbf{B})$  and  $\mathbf{T}_s$ , we define the Task Coverage Region (TCR) of an end-effector pose  $\mathbf{T}_e$  as the set of object poses for which  $\mathbf{T}_e$  lies within their TSRs:

$$\text{TCR}(\mathbf{T}_e) = \{\mathbf{T}_o \mid \mathbf{T}_e \in \text{TSR}(\mathbf{T}_o)\}. \quad (3)$$

Substituting the TSR definition from Eq. 1 yields

$$\text{TCR}(\mathbf{T}_e) = \{\mathbf{T}_e \mathbf{T}_s^{-1} \mathbf{T}_\delta^{-1} \mid \mathbf{T}_\delta \in \Delta(\mathbf{B})\}. \quad (4)$$

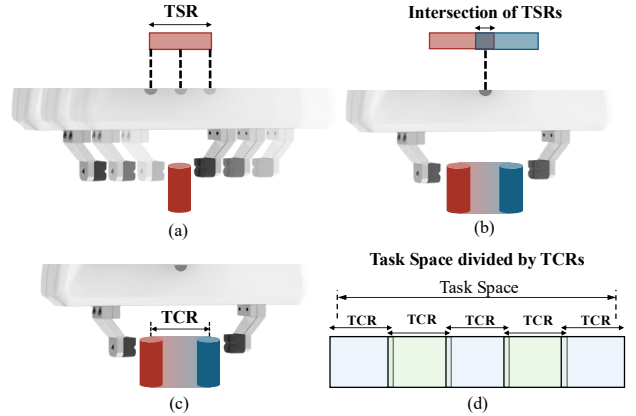


Fig. 3: 2D illustration of TSRs and TCRs.

Intuitively, a TCR describes the region of object poses in  $\mathcal{T}$  for which a fixed end-effector pose  $\mathbf{T}_e$  remains valid. Geometrically, a TCR is obtained by allowing the local offset pose  $\mathbf{T}_\delta$  to vary over the same 6-dimensional box and solving for the corresponding object pose through:  $\mathbf{T}_o = \mathbf{T}_e \mathbf{T}_s^{-1} \mathbf{T}_\delta^{-1}$ . However, due to the inversion this region is not an axis-aligned box in the local coordinates of  $\mathcal{T}$ .

a) *Finite coverage of the task space*: The introduction of TCRs enables us to reduce the continuous task space  $\mathcal{T}$  to a finite set of representative end-effector goals. Specifically, we seek a set of end effector poses  $\{\mathbf{T}_e^i\}_{i=1}^N$  such that every task pose  $\mathbf{T}_p \in \mathcal{T}$  lies within at least one coverage region:

$$\mathcal{T} \subseteq \bigcup_{i=1}^N \text{TCR}(\mathbf{T}_e^i). \quad (5)$$

Each representative end-effector pose  $\mathbf{T}_e^i$  corresponds to an end-effector pose that is valid for all object poses within its task coverage region.

Since TCRs may have irregular shapes and may overlap, to enable constant-time indexing, we discretize the task space  $\mathcal{T}$  into a grid of axis-aligned boxes. Every box should lie entirely inside one TCR to ensure that every task pose  $\mathbf{T}_p$  in the cell can be solved by the corresponding TCR solution pose  $\mathbf{T}_e$ , as in Fig. 3 (d).

We now prove that such a box exists inside every TCR when the TSR bound set  $\Delta(\mathbf{B})$  has non-empty interior. We can conservatively extract such an inner box from each TCR and use the smallest side lengths as a uniform grid size.

**Theorem 1.** *Let  $\Delta(\mathbf{B}) \subset SE(3)$  be the bounded displacement set of TSRs. If  $\Delta(\mathbf{B})$  has non-empty interior, then for any fixed  $\mathbf{T}_e, \mathbf{T}_s \in SE(3)$ ,  $\text{TCR}(\mathbf{T}_e)$  also has non-empty interior and contains an axis-aligned box  $\mathbf{B}_{\text{in}}$ .*

*Proof Sketch.* Define map  $f(\mathbf{T}) = \mathbf{T}^{-1}$ . The inversion is diffeomorphisms on  $SE(3)$ , hence  $f$  is a diffeomorphism and therefore an open map. If  $\Delta(\mathbf{B})$  contains an open set  $U$ , then  $f(U)$  is open and satisfies  $f(U) \subset \text{TCR}(\mathbf{T}_e)$ . Therefore,  $\text{TCR}(\mathbf{T}_e)$  contains an open set and has non-empty interior. Consequently, under the chosen task-space coordinates, it contains an axis-aligned box with non-empty interior.  $\square$

For  $SE(3)$ , deriving such a box from the TSR bound  $\mathbf{B}$  is highly non-trivial. Although  $\Delta(\mathbf{B})$  is defined as a simple box bound, the inversion transformation (Eq. 3) generally distorts the original bound and results in a complicated region.

However, in this work, we focus on a common picking setting in which the task poses' roll and pitch are fixed, and vary only in  $(x, y, z, \psi)$ , where  $\psi$  denotes yaw. In this case, a conservative inner bound for  $\text{TCR}(\mathbf{T}_e)$  can be derived. Let the TSR bounds be  $|\Delta x| \leq b_x$ ,  $|\Delta y| \leq b_y$ ,  $|\Delta z| \leq b_z$ , and  $|\Delta \psi| \leq b_\psi$ . After inversion, the  $(x, y)$  translation components become coupled with yaw and no longer remain axis-aligned. To obtain a yaw-invariant inner bound, we inscribe an axis-aligned square inside the rotated  $(x, y)$  region, and a conservative bound is

$$h_{xy} = \frac{\min(b_x, b_y)}{\sqrt{2}}, \quad |\Delta x| \leq h_{xy}, \quad |\Delta y| \leq h_{xy}. \quad (6)$$

The  $z$  and yaw components remain decoupled from the rotation about the  $z$ -axis and thus retain their original bounds. Combining these bounds yields a conservative axis-aligned inner box  $\mathbf{B}_{\text{in}}$  for the TCR, with widths

$$\delta_x = 2h_{xy}, \quad \delta_y = 2h_{xy}, \quad \delta_z = 2b_z, \quad \delta_\psi = 2b_\psi. \quad (7)$$

Let the bounded task space be  $x \in [x_l, x_h], y \in [y_l, y_h], z \in [z_l, z_h], \psi \in (0, 2\pi]$ . We can map any query pose  $(x, y, z, \psi)$  in task space to a grid index:

$$i_x = \lfloor \frac{x - x_l}{\delta_x} \rfloor, \quad i_y = \lfloor \frac{y - y_l}{\delta_y} \rfloor, \quad i_z = \lfloor \frac{z - z_l}{\delta_z} \rfloor, \quad i_\psi = \lfloor \frac{\psi}{\delta_\psi} \rfloor, \quad (8)$$

where  $\lfloor c \rfloor$  is the floor operator returning the largest integer  $\leq c$ . The tuple  $(i_x, i_y, i_z, i_\psi)$  uniquely indexes a TCR cell and can be used as a key to retrieve end-effector goals and motion solutions.

### B. Offline Library Building with Compression

After task space discretization, a brute-force library would simply plan and store a path for every TCR. This is often impractical due to its large memory footprint.

COAD instead constructs a compressed library by planning root paths for a subset of TCRs, and covering additional TCRs by adapting root solutions, as summarized in Alg. 1. The

---

### Algorithm 1: BuildLibrary( $\mathcal{R}, \mathcal{A}, q_{\text{start}}$ )

---

```

/* Initialize library */
1  $L \leftarrow$  Empty root motion list;
2  $\mathcal{M} \leftarrow$  Empty hash map from a TCR  $r$  to root motion
    $\Pi_{\text{root}}$  and joint goal of the region  $q$ ;
3 while  $\mathcal{R} \neq \emptyset$  do
   /* Sample a new root region */
4    $r \leftarrow$  UniformSampling( $\mathcal{R}$ );
5    $\mathcal{R}.$ Remove( $r$ );
   /* Obtain a root goal in joint space */
6    $q_{\text{root}} \leftarrow$  IK( $r, q_{\text{start}}$ );
7   if  $q_{\text{root}} = \text{null}$  then
8     continue;
   /* Solve for a root path */
9    $\pi_{\text{root}} \leftarrow$  Plan( $q_{\text{start}}, q_{\text{root}}, \mathcal{C}_{\text{free}}(r)$ );
10  if  $\pi_{\text{root}} = \text{null}$  then
11    continue;
   /* Build and store the root motion */
12   $\Pi_{\text{root}} \leftarrow \mathcal{A}.$ BuildRootMotion( $\pi_{\text{root}}$ );
13   $L.$ Append( $\Pi_{\text{root}}$ );
   /* Register the root region as covered by
   this root motion */
14   $\mathcal{M}(r) \leftarrow \Pi_{\text{root}}, q_{\text{root}}$ ;
   /* Try to cover nearby regions via
   adaptation from the same root motion */
15  forall  $r_n \in$  NearestNeighbor( $r, N_{\text{neighbor}}$ ) do
16     $q_n \leftarrow$  IK( $r_n, q_{\text{root}}$ );
17    if  $q_n = \text{null}$  then
18      continue;
19     $\pi_n \leftarrow \mathcal{A}.$ Adapt( $\Pi_{\text{root}}, q_n$ );
20    if IsValidPath( $\pi_n$ ) = true then
21       $\mathcal{M}(r_n) \leftarrow \Pi_{\text{root}}, q_n$ ;
22       $\mathcal{R}.$ Remove( $r_n$ );
23 return  $L, \mathcal{M}$ ;

```

---

algorithm takes TCRs  $\mathcal{R}$ , adaptation method  $\mathcal{A}$  and starting configuration  $q_{\text{start}}$  as input. It initializes an empty root-motion list  $L$  and an empty hash map  $\mathcal{M}$  that associates each region  $r$  with a root motion  $\Pi_{\text{root}}$  and the joint goal of the region  $q$  (line 1-line 2).

While  $\mathcal{R}$  is not empty and we have uncovered regions, the algorithm uniformly samples a region  $r$  from the TCRs  $\mathcal{R}$  as root region and removes it from further consideration (line 3-line 5). It then solves inverse kinematics (IK), warm-started from  $q_{\text{start}}$ , to obtain a root goal configuration  $q_{\text{root}}$  for the task at  $r$  (line 6). If IK fails, the iteration terminates and continues to the next sample (line 7-line 8).

Given a feasible IK goal, a root joint-space path  $\pi_{\text{root}}$  is planned from  $q_{\text{start}}$  to  $q_{\text{root}}$  with free configuration space  $\mathcal{C}_{\text{free}}(r)$  conditioned on the TCR  $r$  (line 9), where collisions account for the swept volume induced by all possible goal poses within  $r$  [14]. In this work, we use RRT-Connect [8] to plan the initial solution and run simplification and smoothing [17] to refine the path. If planning fails, the task is considered infeasible and the algorithm continues to the

next region (line 10-line 11). Otherwise, the resulting root path is converted into a root motion representation  $\Pi_{\text{root}}$  by `BuildRootMotion` of adaptation method  $\mathcal{A}$ , and added to library  $L$  (line 12-line 13). The motion representation is method-dependent. For example,  $\Pi_{\text{root}}$  for linear interpolation is the path  $\pi_{\text{root}}$  itself. Please refer to Sec. IV-C for details. The root region  $r$  is then covered by  $\Pi_{\text{root}}$  conditioned on  $q_{\text{root}}$ , and being registered in the map (line 14).

Finally, the algorithm attempts to expand region coverage by iterating over a set of  $N_{\text{neighbor}}$  nearest neighbors  $r_n$  around the root region (line 15). In this work, we choose  $N_{\text{neighbor}} = 1000$ . For each neighbor, it solves IK, warm-started from  $q_{\text{root}}$ , to obtain a joint goal  $q_n$  of the neighbor region (line 16-line 18). If successful, the adaptation module  $\mathcal{A}$  generates a candidate path  $\pi_n$  by transforming the stored root motion  $\Pi_{\text{root}}$  conditioned on  $q_n$  with method `Adapt` (line 19). If the adapted path can both reach the goal and is collision free, the neighbor region is marked as covered in  $\mathcal{M}$  and removed from  $\mathcal{R}$  (line 20-line 22). When  $\mathcal{R}$  becomes empty, it returns the library  $L$  and the region-to-solution map  $\mathcal{M}$  (line 23).

### C. Adaptation Methods

Given a root path  $\pi_{\text{root}}$ , an adaptation method  $\mathcal{A}$  first generates method-specific root motion  $\Pi_{\text{root}}$  from  $\pi_{\text{root}}$ . Later when a target joint goal  $q_{\text{goal}}$  is provided,  $\mathcal{A}$  transforms the root motion  $\Pi_{\text{root}}$  to a candidate solution  $\pi$ .

All adaptations in COAD are designed to be fast and deterministic. To preserve efficiency, we deliberately *exclude* obstacle avoidance terms from the adaptation objectives. Instead, collision checking is performed during offline verification (line 20 of Alg. 1), ensuring that the adapted path is collision-free. This design introduces a trade-off. Ignoring obstacle constraints, certain neighboring tasks that could otherwise be solved through a heavier optimization process, may no longer be covered. In practice, we find that our methods can still achieve up to 97% compression ratios without obstacle terms (Sec. V-B). Importantly, this design choice substantially accelerates online queries, enabling millisecond-level responses and aligning with the goal of constant-time planning after pre-processing.

Below we introduce three different adaptation strategies, each in terms of its general idea, what is stored as  $\Pi_{\text{root}}$ , and how `Adapt` produces path  $\pi$ .

1) *Linear Interpolation (LI)*: For nearby goals, the simplest adaption strategy is to connect the end of the root path  $q_{\text{root}}$  with the desired goal  $q_{\text{goal}}$  through linear interpolation. Specifically, we construct a waypoint sequence  $\pi_{\text{end}} = \{q_1, \dots, q_{T_{\text{end}}}\}$  of length  $T_{\text{end}}$ , whose first configuration is  $q_1 = q_{\text{root}}$  and whose last configuration is  $q_{T_{\text{end}}} = q_{\text{goal}}$ :

$$q_n = \left(1 - \frac{n}{T_{\text{end}}}\right)q_{\text{root}} + \frac{n}{T_{\text{end}}}q_{\text{goal}}, \quad n \in [1, T_{\text{end}}], \quad (9)$$

and append  $\pi_{\text{end}}$  to the root path  $\pi_{\text{root}}$ . This produces a joint-space path that reaches  $q_{\text{goal}}$  exactly.  $T_{\text{end}}$  can be chosen with desired path resolution. However, this joint path can introduce discontinuities in end-effector motion in the work space. Therefore, we additionally include a continuity verification from [18] in the library building phase. The intuition of the

verification is that, given the joint-space path being a straight line, the end-effector motion in task space should also be nearly a straight line with some threshold.

For this method,  $\mathcal{A}.\text{BuildRootMotion}$  simply stores the root path itself as the root motion representation, i.e.,  $\Pi_{\text{root}} \equiv \pi_{\text{root}}$ .  $\mathcal{A}.\text{Adapt}$ , as described in Eq. 9, takes the root path  $\pi_{\text{root}}$ , builds interpolation sequence  $\pi_{\text{end}}$ , and returns the concatenated path  $\pi_{\text{root}} \parallel \pi_{\text{end}}$ .

2) *Dynamic Movement Primitives (DMPs)*: DMPs provide a compact dynamical system representation of a demonstrated path and allow fast goal retargeting while preserving qualitative shape [19]. Given a path as reference, we model each joint path using a second-order stable dynamical system with a learned nonlinear forcing term:

$$\ddot{q}_i = \alpha_y (\beta_y (g_i - q_i) - \dot{q}_i) + f_i(s), \quad (10)$$

where  $\alpha_y, \beta_y > 0$  are gain hyper-parameters controlling convergence and damping,  $g_i$  is the goal of each joint,  $i$  denotes the joint index, and  $s \in [0, 1]$  is a phase variable for motion progression. The forcing term  $f_i(s)$  is represented as a weighted sum of  $N_B$  fixed basis functions and is learned from the reference path. Compared to appending a terminal interpolation segment, DMPs are slower but can adjust the trajectory globally.

For this method,  $\mathcal{A}.\text{BuildRootMotion}$  fits independent DMPs with  $\pi_{\text{root}}$  to each joint dimension and stores the learned basis weights as the root motion representation  $\Pi_{\text{root}}$ . In contrast to storing all  $T$  waypoints, DMPs require only  $O(N_B)$  parameters per joint. The function  $\mathcal{A}.\text{Adapt}$  performs a forward rollout of Eq. 10 with the goal set to the given  $q_{\text{goal}}$ , producing the adapted trajectory  $\pi$ . The rollout is executed for a fixed number of discrete time steps  $T$ , consistent with the resolution of  $\pi_{\text{root}}$ .

3) *Simple Trajectory Optimization (STO)*: The STO adaptation performs a simplified trajectory refinement inspired by trajectory optimization via sequential convex optimization (TrajOpt) [9], and by the observation that stored motions can serve as effective warm-starts for optimization [11]. Given the stored root path  $\pi_{\text{root}}$  as initialization, we solve a single convex quadratic program that minimizes joint-space velocity and acceleration while penalizing deviation from the stored root path, subject to boundary and joint-limit constraints. Let  $q_{0:T} := (q_0, \dots, q_T)$  denote the path variables, and let  $q_{\text{root},0:T}$  denote the waypoints of the root path. The QP solves:

$$\begin{aligned} \min_{q_{0:T}} \quad & w_v \|D_1 q_{0:T}\|_2^2 + w_a \|D_2 q_{0:T}\|_2^2 + w_s \|q_{0:T} - q_{\text{root},0:T}\|_2^2 \\ \text{s.t.} \quad & q_0 = q_{\text{start}}, \quad q_T = q_{\text{goal}}, \quad q_{\min} \leq q_t \leq q_{\max} \quad \forall t, \end{aligned} \quad (11)$$

where  $w_v, w_a, w_s > 0$  are weighting parameters,  $D_1$  and  $D_2$  denote first- and second-order finite-difference operators along the path,

For this method,  $\mathcal{A}.\text{BuildRootMotion}$  stores the root path  $\pi_{\text{root}}$  as the root motion representation  $\Pi_{\text{root}}$ , which will be used as the initialization and reference trajectory in the QP. The function  $\mathcal{A}.\text{Adapt}$  solves the convex QP in Eq. 11, and returns an optimized path  $\pi$  satisfying the desired new goal  $q_{\text{goal}}$ . In our implementation, the QP is solved with OSQP [20].

#### D. Online Queries

COAD answers an online query by retrieving and adapting a stored root motion from the compressed library, as summarized in Alg. 2. Given a sensed object pose  $\mathbf{T}_o \in \mathcal{T}$ , the procedure first computes its associated TCR index (Eq. 8) to find TCR region  $r$  (line 1). If the index is not covered by the map, the query terminates and returns null, indicating that solution is not available for this problem (line 2 - line 3). Otherwise, the map returns the corresponding root motion  $\Pi_{\text{root}}$  together with the goal joint configuration  $q_{\text{goal}}$  for this problem (line 4). Finally, the adaptation module  $\mathcal{A}$  transforms  $\Pi_{\text{root}}$  into a joint-space path conditioned on  $q_{\text{goal}}$ , producing the solution  $\pi_{\text{sol}}$  (line 5-line 6).

---

#### Algorithm 2: Query( $\mathbf{T}_o, \mathcal{M}, L, \mathcal{A}$ )

---

```

/* Find TCR region */
1  $r \leftarrow \text{GetRegion}(\mathbf{T}_o)$ ;
/* Acquire joint goal and root motion */
2 if  $r \notin \mathcal{M}$  then
3   return null;
4  $\Pi_{\text{root}}, q_{\text{goal}} \leftarrow \mathcal{M}(r)$ ;
/* Apply adaptation */
5  $\pi_{\text{sol}} \leftarrow \mathcal{A}.\text{Adapt}(\Pi_{\text{root}}, q_{\text{goal}})$ ;
6 return  $\pi_{\text{sol}}$ ;

```

---

The online phase therefore reduces planning to a constant-time retrieval followed by lightweight goal-conditioned deformation. The online cost is dominated by two components: (i) TCR indexing and retrieval, and (ii) adaptation cost.

As shown in Eq. 8, the acquisition of TCR index and TCR region  $r$  is a fixed  $O(1)$  cost arithmetic operation, and the retrieval of  $\Pi_{\text{root}}$  from  $\mathcal{M}$  and  $L$  are expected  $O(1)$  with hash lookup and array indexing.

Among the adaptation methods, linear interpolation is  $O(T_{\text{end}})$ , where  $T_{\text{end}}$  is the number of interpolated waypoints from the root end to the desired goal. In this work, we use  $T_{\text{end}} = 10$ . The time complexity of DMP rollout is  $O(T \cdot N_B)$  with fixed  $B$  basis functions and  $T$  generated waypoints. For the optimization-based adapter STO, the runtime scales approximately as  $O(T \cdot I)$ , where  $I$  denotes the maximum number of solver iterations. In motion planning practice, where trajectories are stored at a fixed resolution (in this work,  $T = 200$ ), this yields a predictable fixed runtime. Since all adapter parameters, such as  $T_{\text{end}}, T, N_B$  and  $I$  are fixed offline, the online query stage has constant-time with respect to the online input.

## V. EXPERIMENTS

To assess COAD, we conduct experiments with two robotic manipulators across three simulated environments with varying geometric constraints and planning difficulty, evaluating both offline library quality and online planning performance. We further validate the method in a real-world setting.

### A. Experiment Setup

We evaluate the performance of our method in simulation on two manipulators: Panda (7-DOF) and Fetch (8-DOF) in

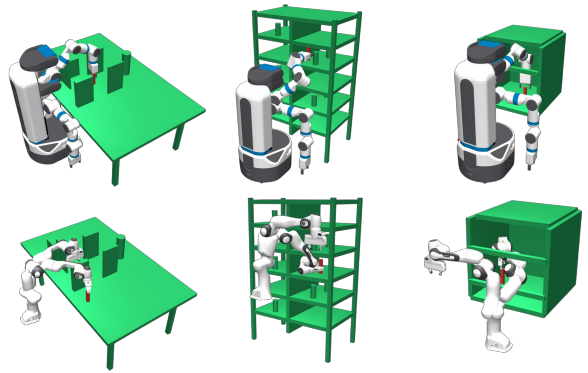


Fig. 4: Fetch (top) and Panda (bottom) manipulators planning in Table (left), Shelf (middle) and Cage (right) environments adapted from [21].

three representative environments: Table, Cage, and Shelf, as demonstrated in Fig. 4 adapted from [21]. We also validate the proposed methods in real world with a physical UR10 robot in a real table environment, as shown in Fig. 1. These environments are designed to reflect different geometric complexity, from open tabletop manipulation (Table), to narrow passages (Shelf), and cluttered obstacle configurations (Cage). The evaluations focus on two key aspects: (i) compression ratio and memory-quality trade-off of the offline plan library, (ii) online planning success rate, efficiency, and path quality.

In this experimental setting, the robots are tasked with reaching a desired end-effector pose corresponding to a grasp pose for the object. Each query specifies a goal pose sampled from the potential task space. In our setting, the static environment obstacles (e.g., table, shelf, cage structure) remain fixed, while the query-dependent object to be grasped varies across tasks. All experiments are conducted in Mujoco simulation on a machine with Intel i7-14700 and 32 GB RAM. Collision checking and kinematic computations are performed using the same geometric models for both offline library generation and online query evaluation.

For each robot-environment pair, we first generate all the TCRs, followed by inverse kinematics (IK) to obtain joint-space goal configurations. For benchmarking purposes, a full solution library is generated by solving and storing each TCR. This full library serves as the uncompressed baseline. Compressed plan libraries are then generated with the three adaptation methods described in Sec. IV-C. We denote them as COAD-LI, COAD-DMP and COAD-STO in the following content. We measure path quality using joint-space path length. For a path waypoint  $\pi = [q_0, q_1, \dots, q_T]$ , we define:

$$L(\pi) = \sum_i \|q_{i+1} - q_i\|_2. \quad (12)$$

### B. Offline Library Building

We first evaluate the compression performance of COAD with three different adaptation methods. Table I summarizes the compression ratio, defined as the percentage reduction in the number of stored paths relative to the full library, together with the average adaptation time and the resulting path quality. For all adaptation methods, COAD achieves a significant reduction in storage requirements. Among

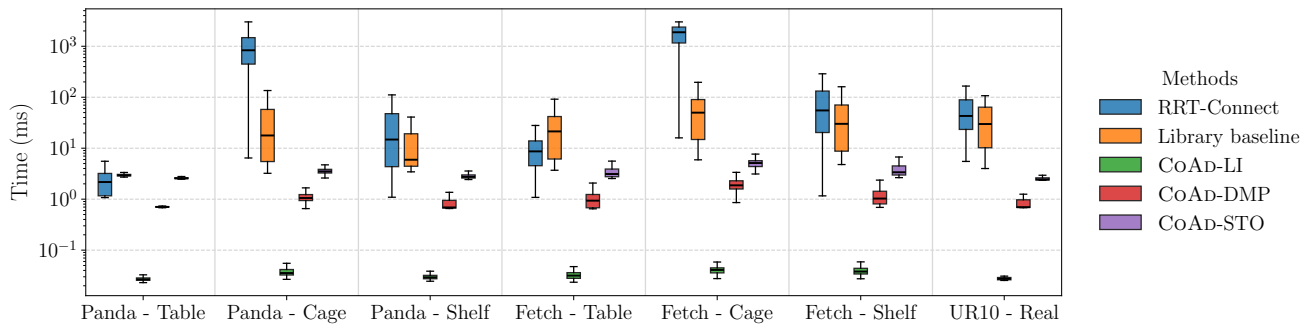


Fig. 5: Comparison of Planning Times for all methods. Y-axis is in log-scale milli-seconds. RRT-connect has a 3.0 second timeout. The library baseline has the same number of paths as the uncompressed COAD.

TABLE I: Plan Library

Env.	Metric	Full Library	COAD-LI	COAD-DMP	COAD-STO
Panda -Table	Comp. (%)	-	97.77	<b>97.91</b>	97.87
	Time (ms)	0.012	<b>0.024</b>	0.721	2.491
	Quality (rad)	2.46	3.20	<b>2.76</b>	3.19
	Size	5033	112	105	107
Panda -Cage	Comp. (%)	-	93.05	74.06	<b>93.36</b>
	Time (ms)	0.013	<b>0.026</b>	1.20	3.40
	Quality (rad)	8.87	9.05	<b>7.99</b>	8.88
	Size	5829	405	1512	387
Panda -Shelf	Comp. (%)	-	97.61	90.39	<b>97.84</b>
	Time (ms)	0.013	<b>0.025</b>	0.869	2.764
	Quality (rad)	5.31	<b>5.39</b>	5.58	5.49
	Size	30013	716	2883	649
Fetch -Table	Comp. (%)	-	87.25	78.98	<b>88.88</b>
	Time (ms)	0.012	<b>0.025</b>	1.058	3.278
	Quality (rad)	7.28	<b>7.34</b>	7.54	7.99
	Size	7646	975	1607	850
Fetch -Cage	Comp. (%)	-	67.89	36.97	<b>72.63</b>
	Time (ms)	0.013	<b>0.028</b>	2.034	5.139
	Quality (rad)	15.70	15.10	<b>14.72</b>	15.18
	Size	844	271	532	231
Fetch -Shelf	Comp. (%)	-	89.93	54.08	<b>90.37</b>
	Time (ms)	0.012	<b>0.030</b>	10.151	3.578
	Quality (rad)	10.02	8.61	<b>7.88</b>	9.01
	Size	33468	3369	15367	3223
UR10 -Real	Comp. (%)	-	89.38	76.76	<b>90.73</b>
	Time (ms)	0.011	<b>0.023</b>	1.009	2.680
	Quality (rad)	7.07	7.04	7.35	<b>7.02</b>
	Size	8676	921	2016	804

the adaptation methods, COAD-STO achieves the highest compression, reducing the library size by 72–99%. COAD-LI achieves similar compression of 67–97%. COAD-DMP compresses less in more constrained environments, but still achieves 50–97% compression across all problems. Among the adaptation methods, COAD-LI has the fastest adaptation time, but this naive adaptation method results in the worst path quality. COAD-DMP displays millisecond-level adaptation times while producing significantly better path quality. These results demonstrate that substantial memory reduction can be achieved without sacrificing task coverage, planning speed or path quality under the varied-goal setting.

### C. Online Planning

We evaluate the online planning performance over 1000 random queries per setting. The quantitative results for success rate and path quality are summarized in Table II. COAD is benchmarked against two baselines: RRT-Connect [8] and a

library-based approach [4]. RRT-Connect is executed with a timeout of 3.0 seconds. We use the library baseline as a representative of the experience-based methods [4]. We construct a library of paths with  $N$  object poses sampled from the task set, where  $N$  matches the size of the full library of COAD for each problem. Unlike COAD, however, this baseline does not discretize the task space and instead store paths by the continuous sampled object poses. For the library baseline, candidate paths are retrieved based on the Euclidean distance between the queried object pose and stored object poses, and the five nearest neighbors are considered. Each retrieved path is adapted using a repair strategy similar to [4]: invalid segments are repaired with RRT-Connect and the path is rewired to the queried goal using linear interpolation, falling back to RRT-Connect if interpolation fails. The first successful adaptation is returned. Otherwise, the query is recorded as a failure.

Across all robot–environment pairs, COAD achieves a 100% success rate, while RRT-Connect and the library baseline occasionally fail in more constrained environments. In terms of path quality, all COAD adaptations outperform RRT-Connect and achieve comparable quality to the library baseline, with COAD-DMP providing the best path quality across all experiments.

Fig. 5 shows the distribution of planning times. COAD significantly outperforms all baselines, achieving up to two orders of magnitude speedup in the open Table environment and nearly three orders of magnitude in more constrained environments such as Cage and Shelf. Among the adaptation methods, COAD-LI is the fastest and requires only constant-time adaptation, as it performs linear interpolation to connect to the new goal. COAD-DMP and COAD-STO achieve planning times on the order of tens of milliseconds while producing higher-quality paths.

### D. Real-world Validation

To validate practical applicability, we evaluate with a UR10 robot in a table scenario as shown in Fig. 1. The compressed library is generated in simulation and transferred directly to the physical system. We assume that the geometry and poses of the fixed obstacles, as well as those of the goal object, are known a priori. During execution, the pose of the goal object is estimated online using an AprilTag-based vision system.

TABLE II: Path Quality and Success Rate

Robot / Env	Metric	RRT-Connect	Library Baseline	CoAD -LI	CoAD -DMP	CoAD -STO
Panda - Table	Success (%)	<b>100</b>	99.90	<b>100</b>	<b>100</b>	<b>100</b>
	Quality (rad)	6.28 ± 2.07	3.10 ± 1.84	3.19 ± 1.12	<b>2.69 ± 1.19</b>	3.13 ± 1.41
Panda - Cage	Success (%)	87.80	90.20	<b>100</b>	<b>100</b>	<b>100</b>
	Quality (rad)	22.18 ± 6.47	10.49 ± 5.21	9.08 ± 2.12	<b>7.98 ± 2.04</b>	8.69 ± 2.12
Panda - Shelf	Success (%)	97.90	98.20	<b>100</b>	<b>100</b>	<b>100</b>
	Quality (rad)	11.80 ± 5.38	5.85 ± 2.31	<b>5.35 ± 1.35</b>	5.65 ± 1.82	5.54 ± 1.39
Fetch - Table	Success (%)	<b>100</b>	64.50	<b>100</b>	<b>100</b>	<b>100</b>
	Quality (rad)	17.23 ± 8.39	7.38 ± 3.94	7.37 ± 3.34	<b>7.29 ± 2.85</b>	7.94 ± 3.51
Fetch - Cage	Success (%)	39.70	49.40	<b>100</b>	<b>100</b>	<b>100</b>
	Quality (rad)	37.11 ± 11.50	16.02 ± 5.66	<b>14.90 ± 4.27</b>	15.01 ± 4.63	15.04 ± 4.78
Fetch - Shelf	Success (%)	98.10	64.50	<b>100</b>	<b>100</b>	<b>100</b>
	Quality (rad)	21.29 ± 11.01	9.97 ± 6.15	8.81 ± 4.37	<b>8.50 ± 3.95</b>	8.77 ± 4.63
UR10 - Real	Success (%)	<b>100</b>	85.00	<b>100</b>	<b>100</b>	<b>100</b>
	Quality (rad)	17.19 ± 6.96	8.38 ± 4.46	8.17 ± 5.11	<b>7.38 ± 4.70</b>	8.29 ± 4.52

We randomly placed the goal object within the predefined task space for 20 trials. The observed performance trends, including success rates, query time, and path quality, are consistent with the simulation results and are reported in Fig. 5 and Table II. This demonstrates that the proposed framework is applicable in real robotic systems.

## VI. CONCLUSION AND FUTURE WORK

In this paper, we present COAD, a framework for goal-varying manipulation planning that combines task-space discretizations via TCRs, offline construction of a compressed library, and efficient online adaptation. By shifting the majority of the planning and adaptation verification effort to an offline phase, COAD enables constant-time query while significantly reducing memory requirements.

Currently, the root regions are randomly selected. A promising direction for future work is to design more representative root-selection algorithms to further minimize the number of root paths required. Another important extension is to relax the semi-static assumption and build a motion library suitable for more general semi-static environments, which includes both varying goals and moving obstacles [14].

## REFERENCES

- [1] H. Choset, K. M. Lynch, S. Hutchinson, G. A. Kantor, and W. Burgard, *Principles of robot motion: theory, algorithms, and implementations*. MIT press, 2005. <https://ieeexplore.ieee.org/servlet/opac?bknumber=6267238>
- [2] K. E. Bekris, J. Doerr, P. Meng, and S. Tangirala, "The state of robot motion generation," *arXiv preprint arXiv:2410.12172*, 2024. <https://arxiv.org/abs/2410.12172>
- [3] H. Ishida, N. Hiraoka, K. Okada, and M. Inaba, "Coverlib: Classifiers-equipped experience library by iterative problem distribution coverage maximization for domain-tuned motion planning," *IEEE Trans. Robot.*, 2025. <https://ieeexplore.ieee.org/document/10930729>
- [4] D. Berenson, P. Abbeel, and K. Goldberg, "A robot path planning framework that learns from experience," in *IEEE Intl. Conf. Robot. Autom.*, 2012, pp. 3671–3678. <https://ieeexplore.ieee.org/document/6224742/>
- [5] D. Coleman, I. A. Şucan, M. Moll, K. Okada, and N. Correll, "Experience-based planning with sparse roadmap spanners," in *IEEE Intl. Conf. Robot. Autom.*, 2015, pp. 900–905. <https://ieeexplore.ieee.org/abstract/document/7139284>
- [6] F. Islam, O. Salzman, A. Agarwal, and M. Likhachev, "Provably constant-time planning and replanning for real-time grasping objects off a conveyor belt," *Intl. J. of Robotics Research*, vol. 40, no. 12-14, pp. 1370–1384, 2021. <https://doi.org/10.1177/02783649211027194>
- [7] L. E. Kavraki, M. N. Kolountzakis, and J.-C. Latombe, "Analysis of probabilistic roadmaps for path planning," *IEEE Trans. Robot.*, vol. 14, no. 1, pp. 166–171, 1998. <https://ieeexplore.ieee.org/document/660866>
- [8] J. Kuffner and S. LaValle, "Rrt-connect: An efficient approach to single-query path planning," in *IEEE Intl. Conf. Robot. Autom.*, vol. 2, 2000, pp. 995–1001 vol.2. <https://ieeexplore.ieee.org/document/844730>
- [9] J. Schulman, J. Ho, A. Lee, I. Awwal, H. Bradlow, and P. Abbeel, "Finding locally optimal, collision-free trajectories with sequential convex optimization," in *Robotics: Science and Syst.*, 2013. <http://www.roboticsproceedings.org/rss09/p31.pdf>
- [10] N. Ratliff, M. Zucker, J. A. Bagnell, and S. Srinivasa, "Chomp: Gradient optimization techniques for efficient motion planning," in *IEEE Intl. Conf. Robot. Autom.*, 2009, pp. 489–494. <https://ieeexplore.ieee.org/document/5152817>
- [11] T. S. Lembono, A. Paolillo, E. Pignat, and S. Calinon, "Memory of motion for warm-starting trajectory optimization," *IEEE Robot. Autom. Letters*, vol. 5, no. 2, pp. 2594–2601, 2020. <https://ieeexplore.ieee.org/abstract/document/8990042>
- [12] C. Chamzas, Z. Kingston, C. Quintero-Peña, A. Shrivastava, and L. E. Kavraki, "Learning Sampling Distributions Using Local 3D Workspace Decompositions for Motion Planning in High Dimensions," in *IEEE Intl. Conf. Robot. Autom.*, June 2021, pp. 1283–1289. <https://dx.doi.org/10.1109/ICRA48506.2021.9561104>
- [13] F. Islam, C. Paxton, C. Eppner, B. Peele, M. Likhachev, and D. Fox, "Alternative paths planner (app) for provably fixed-time manipulation planning in semi-structured environments," in *IEEE Intl. Conf. Robot. Autom.*, 2021, pp. 6534–6540. <https://ieeexplore.ieee.org/abstract/document/9561563>
- [14] N. K. Ilampooranan and C. Chamzas, "Cover: Coverage-verified roadmaps for fixed-time motion planning in continuous semi-static environments," *arXiv preprint arXiv:2510.03875*, 2025. <https://arxiv.org/abs/2510.03875>
- [15] J. P. Van Den Berg and M. H. Overmars, "Roadmap-based motion planning in dynamic environments," *IEEE Trans. Robot.*, vol. 21, no. 5, pp. 885–897, 2005. <https://ieeexplore.ieee.org/document/1512347>
- [16] D. Berenson, S. Srinivasa, and J. Kuffner, "Task space regions: A framework for pose-constrained manipulation planning," *Intl. J. of Robotics Research*, vol. 30, no. 12, pp. 1435–1460, 2011. <https://journals.sagepub.com/doi/10.1177/0278364910396389>
- [17] I. A. Şucan, M. Moll, and L. E. Kavraki, "The Open Motion Planning Library," *IEEE Robot. Autom. Magazine*, vol. 19, no. 4, pp. 72–82, December 2012. <https://ompl.kavrakilab.org>
- [18] Z. Zhong, Z. Li, and C. Chamzas, "Expansion-GRR: Efficient generation of smooth global redundancy resolution roadmaps," in *IEEE/RSJ Intl. Conf. on Intell. Robots and Syst.*, 2024, pp. 8854–8860. <https://ieeexplore.ieee.org/document/10801917/>
- [19] M. Saveriano, F. J. Abu-Dakka, A. Kramerberger, and L. Peternel, "Dynamic movement primitives in robotics: A tutorial survey," *Intl. J. of Robotics Research*, vol. 42, no. 13, pp. 1133–1184, 2023. <https://doi.org/10.1177/02783649231201196>
- [20] B. Stellato, G. Banjac, P. Goulart, A. Bemporad, and S. Boyd, "OSQP: an operator splitting solver for quadratic programs," *Mathematical Programming Computation*, vol. 12, no. 4, pp. 637–672, 2020. <https://doi.org/10.1007/s12532-020-00179-2>
- [21] C. Chamzas, C. Quintero-Peña, Z. Kingston, A. Orthey, D. Rakita, M. Gleicher, M. Toussaint, and L. E. Kavraki, "Motionbenchmarker: A tool to generate and benchmark motion planning datasets," *IEEE Robot. Autom. Letters*, vol. 7, no. 2, pp. 882–889, Apr. 2022. <https://dx.doi.org/10.1109/LRA.2021.3133603>